IEEE Access
Multidisciplinary | Rapid Review | Open Access Journal

Received October 28, 2020, accepted November 7, 2020, date of publication December 7, 2020,
date of current version December 21, 2020.

Digital Object Identifier 10.1109/ACCESS.2020.3042935

Influence of Phase-Shifted Square Wave Modulation on Medium Frequency Transformer in a MMC Based SST

RACHIT AGARWAL, (Student Member, IEEE), SANDRO MARTIN, (Student Member, IEEE), AND HUI LI, (Fellow, IEEE)
Center for Advanced Power Systems, Florida State University, Tallahassee, FL 32310, USA
Corresponding author: Rachit Agarwal (ra15f@my.fsu.edu)

ABSTRACT This article proposes an approach to identify intrinsic power losses of the medium frequency transformer that interfaces two modular multilevel converters (MMC) operated with phase-shifted square wave modulation (PS-SWM) to form a DC solid state transformer (DC SST) module. Cascaded MMC module based DC SST architecture is an excellent choice for HVDC to MVDC conversion for DC grid application as well as for renewable and distributed energy resource integration into the DC grid. Operation with PS-SWM allows reduced cell capacitor size and lower total semiconductor device ratings. However, this modulation generates a unique quasi-square waveform at the SST internal medium frequency (MF) AC interface, which differs from other known square-wave modulation types. This produces a similarly unique transformer flux density, resulting in a transformer core loss that cannot be predicted by existing methods which makes it challenging to identify. In the interest of presenting a useful and optimizable MF transformer design methodology, this article develops a tool to predict the loss of the MF transformer subjected to PS-SWM. The proposed loss estimation technique is validated through an experimental testbed operated in two different configurations and is demonstrated to provide a valid basis for the use of the proposed MF transformer design methodology. Furthermore, this article provides an analysis of the load-dependent MF transformer core loss, which demonstrates a secondary usefulness of the proposed loss prediction tool in identifying load-dependent converter losses

INDEX TERMS Modular multilevel converter (MMC), DC solid state transformer (DC SST), medium frequency transformer (MFT), HVDC to MVDC conversion, DC grid, distributed energy resource (DER) integration, phase shifted square wave modulation (PS-SWM).

I. INTRODUCTION

High voltage isolated bidirectional DC solid state transformers (HV_IBDC) have been an active topic of research in both industry and academia because of the advantages associated with DC transmission and DC distribution. HV_IBDC is a fundamental building block of many AC-AC and DC-DC solid state transformers (SST) [1]–[4]. HV_IBDC is also applied to interconnect HVDC to HVDC or MVDC grids at different voltage levels [5], [6]. Moreover, high voltage power semiconductor technology is now feasible for medium frequency switching which significantly reduces the size and weight of converters. This increases the adaptability of HV_IBDC converters in shipboard applications as well [7], [8]. Fig. 1 shows the application of HV_IBDC as a building block of a DC grid. The MF AC-link transformer is the key element of HV_IBDC converter. MF transformer design is a multidisciplinary task where the transformer, topology and modulation must be taken into consideration. The design and size of the transformer can directly be linked to the frequency and amplitude of AC voltage. In a DAB-Type MVDC-LVDC solid state transformer, Baek *et al.* have presented a 10 kW/ 20 kHz coaxially wound transformer [9]. In this paper the design has been optimized to integrate the DAB's energy transfer inductance into the MF transformer. Thus, the inductance requirement by the DAB circuit is fulfilled by the leakage inductance of the MF transformer and the need for additional inductor hardware is

The associate editor coordinating the review of this manuscript and approving it for publication was Jing Bi.

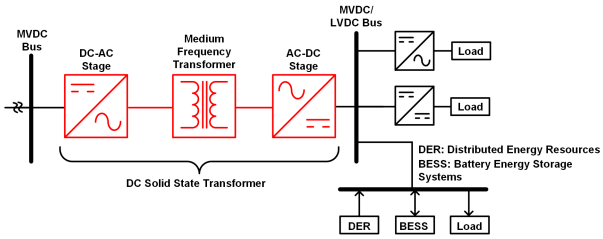

FIGURE 1. HV_IBDC as a DC grid building block.

eliminated. Zhao *et al.* [10] have designed a 15 kW / 50 kHz MF transformer for a CLLC resonant converter module in a MV to LV conversion system. They have achieved a power density of 40.54 kW/l and have rated the isolation voltage at 30 kV. They optimized their transformer design for efficiency and have demonstrated 99.5% peak efficiency. Another transformer design from Chen *et al.* for an LLC module in a MV - LV SST is presented in [11] where the transformer design is optimized for insulation. Basic insulation level (BIL) was tested experimentally upto 95 kV in this design. All the above transformer designs are for the MV-LV SST applications. For HVDC-HVDC or HVDC-MVDC applications, modular multilevel converter (MMC) based topologies are often adopted. Gowaid *et al.* [5] have proposed a HV_IBDC as point-to-point link between two HVDC transmission systems commissioned at different voltage levels. This DC-DC converter is based on the modular multilevel converter (MMC) topology with a 600 MW / 250 Hz AC-link transformer. Another HVDC-MVDC converter with the AC-link transformer requirement of 200 MW / 200 Hz is proposed by Cui *et al.* [6] and Kenzelmann *et al.* [12] have presented a MVDC-MVDC converter with an AC-link of 360 kW/ 1 kHz. The importance of accurate loss prediction to optimize the thermal design of MF transformer is presented in [13]. Although HVDC and MVDC studies have addressed transformer design considerations [5] to enhance system's performance, the actual AC-link transformer design and loss analysis needs to be investigated.

In this paper, the effect of PS-SWM modulation on MF transformer is investigated in a 6 kV/100 kW MMC based SST module. The converter modules are connected in Input-Series-Output-Parallel (ISOP) configuration to form a mega-watt scale SST architecture to interface HVDC and MVDC grids. The system configuration is shown in Fig. 2. This converter module provides galvanic isolation between the HV and MV side and allows bidirectional power flow. This makes this converter a suitable candidate for large scale energy storage system and PV systems application on the MV DC bus. In a previous work, [14], [15] a phase shifted square wave modulation (PS-SWM) is proposed that has shown that the converter can provide comparable DC filtering with smaller cell capacitors and arm inductors along with a lower total device rating of semiconductor devices. Use of PS-SWM modulation thus aids in achieving higher power density of the SST modules and has shown superior fault control capability as well [8].

The transformer design and optimization for PS-SWM modulation is challenging because of the quasi-square AC voltage excitation with high frequency staircase levels. The transformer loss is compared to pure square wave modulation in [16]. The transformer design for the converter module as a standalone converter for shipboard application is presented in [17]. Since the modulation directly impacts core loss, the transformer core design and core losses are analyzed in detail in this paper. One down-scaled modular multilevel converter SST module and transformer prototype is built in the lab and the core losses are experimentally measured. The measured core loss results are found consistent with the loss predicted by analysis. Therefore, the contributions of this article are listed as follows:

1) High voltage isolated and bi-directional SST module operating with phase-shifted square wave modulation is elucidated and its application in an HVDC to MVDC SST is presented in Section II.
2) MF transformer core loss with PS-SWM is calculated and combined with winding loss. A conceptual design of a 100 kVA transformer is presented achieving high efficiency and power density in Section III.
3) Experimental results obtained from a MMC based SST testbed developed in lab are presented to validate the core loss calculation method in Section IV.
4) Using the validated core loss calculation method from the previous sections, core loss under loaded condition with phase-shifted AC voltage is calculated in Section V.

II. SST ARCHITECTURE WITH PHASE SHIFTED SQUARE WAVE MODULATION

The SST architecture with MMC modules is shown in Fig. 2. Each module consists of two modular multilevel converters (MMCs) with the AC ports connected together by a MF AC-link transformer. Considering power flow from HVDC port to MVDC port, the primary side MMC converter forms the inverter circuit that produces the AC link voltage that is subjected to the MF AC-link transformer. The secondary side MMC converter then actively rectifies the AC voltage to support the MVDC grid. Each phase-leg $'a$ & b' on each side contains 2 arms: positive $'p'$ and negative $'n'$ and each arm contains $'N'$ number of half-bridge cells. Since primary side is connected to the HVDC grid, it is represented as high side $'h'$ and the secondary side supports the MVDC grid hence represented as low side $'l'$. An impedance is placed in series with the primary winding which acts as the power transfer element. The AC-link transformer's leakage inductance L_{ac} is often exclusively utilized as the power transfer element but an additional inductance may be added in series if needed. The power transfer is achieved by inserting a phase-shift between the primary side and secondary side voltages. The direction of power flow depends on the direction of phase-shift angle $'\phi'$. In Fig. 3 secondary side AC voltage $V_{ac,sec}$ is leading with respect to $V_{ac,pri}$. This results in power transfer the

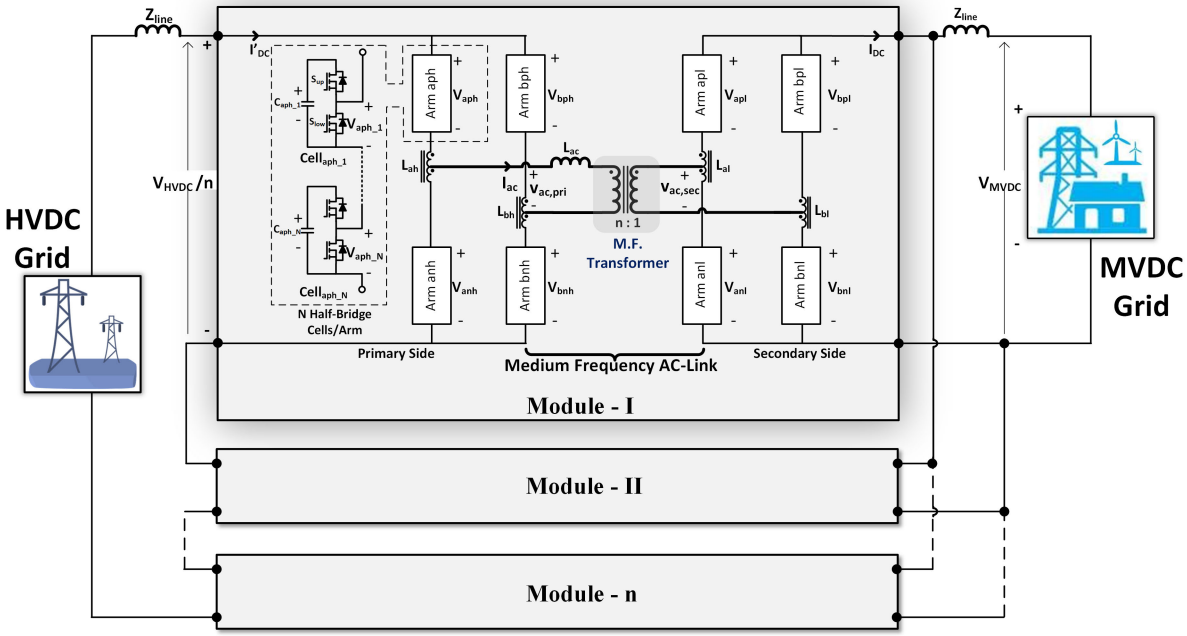

FIGURE 2. MMC module stack based HVDC-MVDC converter.

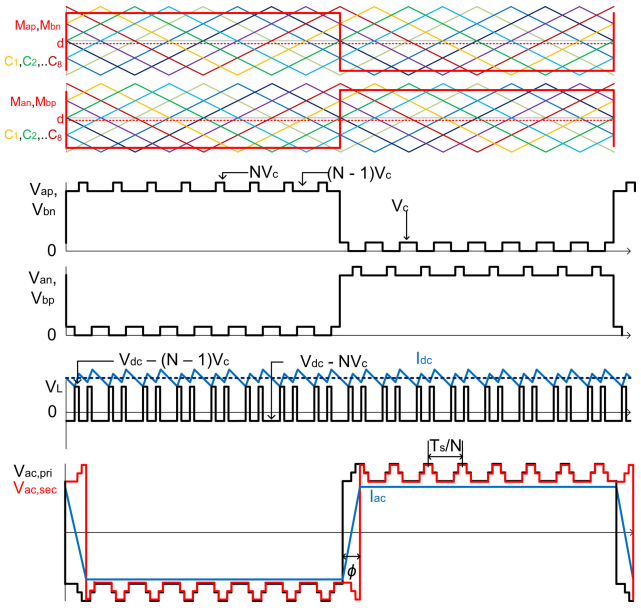

FIGURE 3. Key AC waveforms in PS-SWM modulation.

HVDC port to the MVDC port. Similarly if $V_{ac,sec}$ is lagging $V_{ac,pri}$, the power is transferred from the MVDC port to the HVDC port. The input and output voltage filtering is provided by the cell capacitors present in each half-bridge cell. This eliminates the need of bulky HV capacitors across the input and output ports of the converter thereby reducing the cost and increasing the power density of the system.

The number of cells per arm $'N'$ is determined by the individual bridge's voltage level and the semiconductor device's voltage ratings. Multiple devices in parallel can be used to obtain the desired current capability of the system. To attain high switching frequency and low switching losses while maintaining rugged operation, N = 8 cells/arm is selected. This facilitates the use of MOSFETs to utilize the switching loss benefits over IGBTs in the circuit. The converter module parameters are listed in Table 1.

TABLE 1. iM2DC module circuit parameters.

Parameter	Symbol	Value
Power Rating	P	100 kW
Input Voltage	V_{HVDC}/n	6 kV
Output Voltage	V_{MVDC}	6 kV
Number of cells/arm	N	8
Cell Capacitance	C_{cell}	20 μF
Modulation Index	M	0.8
Modulation DC Offset	d	-0.04
Switching Frequency	f_s	100 kHz
Transformer Turns Ratio	n	1:1
AC-link Frequency	f_{ac}	50 kHz

Sinusoidal modulation and square wave modulation are the two popular modulation methods for the MMC converter. Square wave modulation exhibits improved performance over sinusoidal modulation in terms of power transfer and lower converter rms current flow in the circuit due to better voltage utilization ratio [18]. The rms values of voltage and current in sinusoidal modulation are $\sqrt{2}$ times smaller than square voltage and current. Greater rms voltage and current in square wave modulation allows for a larger power transfer between

the primary and secondary bridges for the same phase-shift angle and input voltage level as compared to sine wave modulation. Smaller rms current at a particular power level in square wave modulation renders lower overall conduction losses in the system, whereas for the same power sinusoidal modulation will require higher rms current resulting in higher conduction losses.

The MMC converter module in the SST architecture is modulated by Phase Shifted Square Wave Modulation (PS-SWM) [14]. PS-SWM allows reduction in the cell capacitor size and in the total device rating (TDR) of the semiconductor switches. Superior current control capability is maintained with smaller passive components in the iM2DC converter which is challenging in HVDC-MVDC converters. The switching frequency f_{sw} is the frequency of triangular carrier waves while the AC-link frequency f_{ac} is equal to the frequency of the square modulation wave. To allow power transfer between bridges, a phase-shift between the primary side and secondary side transformer voltages is inserted by phase-shifting the modulation waves by an angle $\phi°$ between the primary side and secondary side. Fig. 3 shows the primary-side modulation, the primary-side arm voltages, the primary-side arm inductor waveform, and the transformer primary and secondary AC waveform for N=8 cells/arm and $f_{sw} = 2 \cdot f_{ac}$. The peak AC voltage is greater than the input voltage since the cell capacitor voltage is boosted when modulation offset d is negative as indicated by Eq. 1. The peak voltage (first level) is given by $N \cdot V_c$, the second level is at $(N-1) * V_c$ and the third level is at $(N-2) \cdot V_c$ [14], [15], [19].

$$V_c = \frac{U'_{in}}{N(1-d)} \tag{1}$$

III. PS-SWM EFFECT ON TRANSFORMER LOSSES

To analyze the effect of PS-SWM modulation on the transformer design, the losses incurred at the MF transformer are identified. Since the voltage waveform is unique to the modulation scheme and the converter topology, preexisting transformer loss estimation methods needs to be thoroughly investigated and verified. The effect of the modulation on transformer loss is separated into two categories:

(A) Effect on core losses
(B) Effect on winding losses

A concept design for an 100 MVA transformer prototype is also presented at the end of this section. The design is achieves optimal efficiency and power density while maintaining cost balance.

A. EFFECT ON CORE LOSS

The AC voltage excitation waveform applied to the MF transformer is unique to the PS-SWM modulation. Therefore, traditional core loss estimation methods needs to be thoroughly evaluated and verified to make sure that correct estimation is achieved. The methods of core loss calculation are based on breaking up the core loss into three components: Hysteresis Loss, Eddy Currents Loss and Residual Losses [20], [21]. The Eddy current losses are produced by the Eddy currents induced in the conductive magnetic core. Eddy currents are significantly reduced in practice by increasing the resistance of the core through lamination of thin magnetic material layers that forms the core. Studies in [21] have shown that the residual losses are mainly due to magnetic relaxation. Magnetic relaxation occurs when the AC voltage contains a dead-time where it remains zero for a short time interval before changing polarity. Since the AC voltage in PS-SWM with 8 cells/arm does not have a dead-time, the residual losses will not have a significant impact on the total core loss for the selected configuration. Hysteresis loss depends on the peak flux density and increases linearly with frequency. Hence, having the most impact on high frequency power electronic magnetics. Due to this, the core loss due to hysteresis with PS-SWM modulation is discussed in this section.

Core material with high flux density and relative permeability is essential for high voltage and high frequency applications. Nanocrystalline soft magnetic alloy F3CC [22] is selected for the MF transformer core material because of its superior performance in high frequency and high voltage applications [23]. The saturation flux density of F3CC is 1.23 T. This supports greater power density of the transformer and lower hysteresis loss at high frequency. The core material exhibits very high electrical resistance due to very thin 15-25 μm ribbon lamination which greatly reduces the eddy current losses. Furthermore, this material exhibits good thermal performance [13]. The flux density for the applied voltage is calculated by Eq. 2. Fig. 4 shows a piece-wise linear flux density (blue) calculated for the AC-link voltage (red). The edges of the flux density waveform are distorted because of the high frequency voltage ripple on the AC voltage. The edges will become smoother with the increase in $'N'$ because by increasing $'N'$, the difference between the voltage levels decreases, according to Eq.1. For a case when N = 2cells/arm, the flux density at the third voltage level $(N-2) \cdot V_c$ will be flat with no slope because for $N = 2$, the third voltage level becomes 0. This is an edge case where the AC voltage will have a short dead time and residual losses will be generated.

Ferrite core material was also evaluated for the MF transformer design but was rejected due to its lower saturation

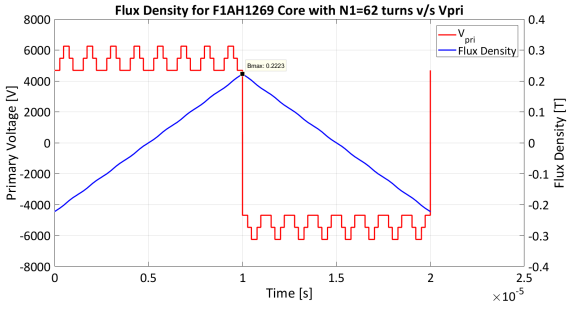

FIGURE 4. AC voltage vs. flux density.

flux density B_{sat} as compared to nanocrystalline core material. A lower B_{sat} means that a larger Ferrite core would be required with a greater number of winding turns. This will increase the overall power loss and weight of the AC-link transformer.

Fabricating the AC-link transformer with F3CC core material in uncut UU shape allows for a smaller build volume, lower weight, less winding loss due to reduced winding length, extended operating temperature range and more robust performance. Suitable off the shelf Finemet F3CC core sizes were analyzed to identify the best core size based on maximum efficiency.

$$B(t) = \int_0^T \frac{1}{N_t \cdot A_e} \cdot \frac{dV_{ac}}{dt} \tag{2}$$

where:
N_t = number of primary turns
A_e = cross-section area of the core
V_{ac} = primary side AC-link voltage

The classic Steinmetz's equation for core loss calculation has been extensively proved accurate for sinusoidal voltage excitation. Since the AC voltage produced by this topology and modulation is non sinusoidal, the results obtained by Steinmetz's equation are unreliable. Therefore Improved General Steimmetz Equation (iGSE) [24] is used which is suitable for non-sinusoidal voltages. A complete cycle of voltage and current is simulated with a fine time step of 5 ns to achieve accurate computation of loss results. To identify the best core geometry, the maximum flux density and core loss for all off the shelf core geometries are calculated. The calculations are based on maximum possible number of winding turns for a 1:1 turns ratio while leaving clearance for insulation and other accessories. Using Eq. 3 and Eq. 4 the core loss densities for all available core geometries is calculated.

$$\overline{P_v} = \frac{1}{T}\int_0^T k_i \left|\frac{dB}{dt}\right|^{\alpha} (\Delta B)^{\beta-\alpha} \tag{3}$$

$$k_i = \frac{k}{(2\pi)^{\alpha-1}\int_0^{2\pi} |cos\theta|^{\alpha}\, 2^{\beta-\alpha} d\theta} \tag{4}$$

where:
B = instantaneous flux density
ΔB = peak to peak amplitude change in flux density
α, β, k = Steinmetz coefficient

Fig. 5 shows a plot that compares maximum flux density B_{max} vs. the core cross section area A_e. The maximum value of flux density is then found by piecewise linear analysis like the plot shown in Fig. 4. The transformer configuration where $B_{max} > B_{sat}$ is rejected because the operating magnetic field exceeds the practical limitation of the core material. After finding the array of flux densities for available cores, the core loss density is calculated by using Eq. 3 and Eq. 4 with a help of a piece-wise linear manner. The specific core loss can then be calculated for each core by multiplying its

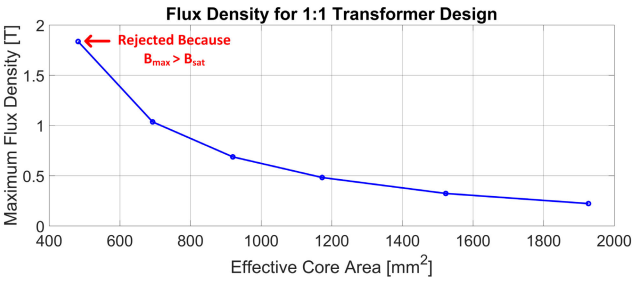

FIGURE 5. Maximum flux density vs. core cross-section area.

core loss density P_v with the core weight. Fig. 6 shows the value of calculated core loss v/s area of cross section of core A_e. From this graph, the core with the smallest specific core loss is identified. It should be noted that the core material data sheet is not one hundred percent accurate and there can be small error in Steinmetz parameters This difference will reflect in the real and calculated core loss figure. Datasheet derived Steinmetz parameters for the core material, the calculated maximum flux density and the calculated core loss density for the chosen core geometry are listed in Table 2.

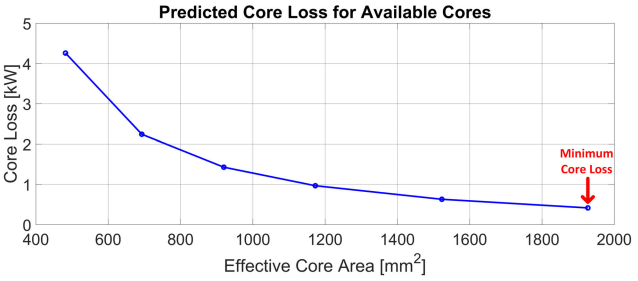

FIGURE 6. Core loss vs. core cross-section area.

TABLE 2. Core material parameters and calculated core loss density.

Parameter	Value
Core Material	$Finemet\ F3CC$
α	1.583
β	2.0861
k	4.422×10^{-8}
A_e	$1927\ mm^2$
$B_{max\,PS-SWM}$	$0.2512\ T$
$P_{v\,PS-SWM}$	$61.5\ W/kg$

B. WINDING LOSS

The rectified current produced by the primary side of the MMC module is assumed to be pure square because the switching frequency features are substantially diminished by the AC inductance in the circuit. Foil-type conductors are widely accepted in high frequency, high power transformer

because of their relatively larger cross sectional area [25]. This keeps the maximum current density under acceptable limits. To determine adequate winding geometry, the required winding cross-sectional area for the maximum rated power of the converter is obtained. For 100 kW operation, rms current of 16.7 A must be passing through the 1:1 transformer windings. For copper, current density of $J = 500\ A/cm^2$ is used. The winding cross section area is obtained according to Eq.5 is $A_w = 4\ mm^2$.

$$A_w = \frac{I_{rms}}{J} \tag{5}$$

Electrical grade copper foil is selected as the winding material because of its known benefits over standard copper magnetic wire for high power, high frequency application. The UU core shape and F3CC core material was evaluated with copper foil winding and it was found that with copper foil, adequate packing factor can be achieved. To carry the maximum rms current on each side, $I_{rms} \approx 16.7A$, foil thickness of 5 mil is selected considering skin depth at 50 kHz AC-link frequency. Polyimide insulation (Kapton tape) is then applied over the winding to provide basic insulation. The thickness of self-adhesive polyimide tape is $\approx 5\ mil$ with a dielectric strength of $> 7\ kV/mil$. The maximum number of turns on each side of 1:1 transformer is calculated by using Eq. 6. The constant (9/20) in Eq. 6 incorporates 10% clearance in usable window width given by measurement B_{core} for each core size. This allows for clearance between winding turns and additional insulation requirements.

$$N1 = N2 = \frac{9}{20} \cdot \frac{B_{core}}{t_w + t_i} \tag{6}$$

where:

$N1$ = Number of turns on primary
$N2$ = Number of turns on secondary
B_{core} = Width of the core window [m]
t_w = Thickness of foil [m]
t_i = Thickness of kapton tape insulation [m]

For every identified core geometry, the winding height and number of turns for a 1:1 ratio is calculated. Using this information, the winding loss is obtained for every transformer design with different core and winding geometries. First, the DC resistance of each winding is calculated by using Eq. 7. Height of the copper foil is based on the height of the core window given by C_{core}. The foil is constructed to allow for 10% margin in core height for coil formers, insulation, and other accessories. This margin is represented in Eq. 7 by inserting a constant multiple of 0.9 to the denominator of the expression.

$$R_{dc} = \frac{l_w \cdot N}{t_w \cdot \sigma \cdot 0.9 C_{core}} \tag{7}$$

where, l_w is the length of middle layer of winding, N is the number of turns on each side, t_w is thickness of 1 winding layer, σ is the electrical conductivity of copper and C_{core} is height of core window.

The influence of skin and proximity effects on the ac resistance of transformer windings is estimated by using Dowell's expression [26]. The AC-link current is square in PS-SWM modulation, hence it is assumed that $I_{rms} = I_{peak}$. Based on copper's linear characteristics, the winding losses are calculated by using the harmonic contents of the applied current. The first five dominant harmonic components are identified from the whole spectrum and their respective magnitude and frequency is used to estimate relation factor (RF) for Rac estimation using Eq. 8. After obtaining the RF, the total loss for each winding design is calculated by Eq. 9. Fig. 7 shows calculated winding loss vs number of turns. In this calculation, the height and number of winding turns is varied according to the size of the core window as explained in the previous subsection. The copper foil width is kept constant at 5 mil for all designs because winding cross-sectional area requirement was satisfied with 5 mil thickness for all winding heights ranging from the smallest to the largest core.

$$RF(n) = \Delta\left[\varsigma_1 + \left(\frac{h_w}{B_{core}}\right)^2 \frac{2}{3}(N1^2 - 1)\varsigma_2\right] \tag{8}$$

$$Loss_{wdg} = \sum_{n=1}^{5} I_{RMS}(n)^2 \cdot (RF(n) \cdot R_{dc}) \tag{9}$$

where:

$\Delta = \frac{t_w}{\delta} \cdot \sqrt{\frac{h_w}{B_{core}}}$
δ = Skin depth $= \sqrt{\frac{1}{\pi \mu \sigma f}}$
ς_1 = Skin effect factor $= \frac{sinh(2\Delta) + sin(2\Delta)}{cosh(2\Delta) - cos(2\Delta)}$
μ = Permeability of winding material (copper)
ς_2 = Proximity effect factor $= \frac{sinh(2\Delta) - sin(2\Delta)}{cosh(2\Delta) + cos(2\Delta)}$
h_w = Width of the foil [m]

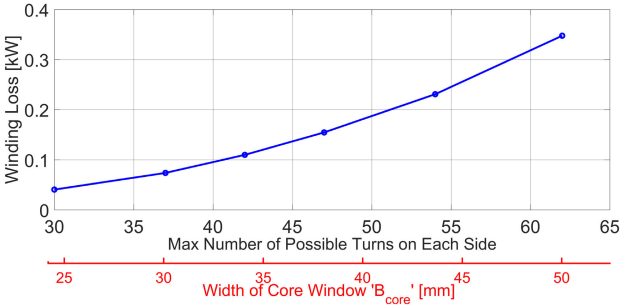

FIGURE 7. Calculated winding loss.

Dowell's expression for estimating ac losses in foil winding has been experimentally evaluated by Bahmani *et al.* in [27]. In this paper they have shown that for porosity factor greater than 0.8, accuracy of Dowell's expression is ±15%, which is acceptable deviation for an analytical tool. Porosity factor is defined as the ratio of core window height occupied by the copper foil to the total window height. Porosity factor for the designed winding is 0.9 and Δ is between 1-2. Thus it

is safe to consider the analytically obtained winding loss to be accurate.

C. FINAL TRANSFORMER DESIGN

By combining the core loss and winding loss results from previous sections, the total AC-link power loss is determined and shown in Fig. 8. The core and winding combination with minimum total power loss is selected as the final design. The total loss is calculated and found to be equal to 763 W making the MF transformer efficiency $\eta = 99.23\%$. Fig. 9 shows the mechanical design of the proposed core-type transformer prototype constructed with nanocrystalline F3CC core and copper foil windings. Constructing the MF transformer in core-type configuration allows better window utilization ratio and smaller core size requirement than shell-type construction. The final specification are listed in Table 3. The total weight of the transformer is calculated by adding the weight of the core from the datasheet and the weight of the copper winding using the density of copper. Weight for insulation, coil former, connectors are also added in the weight calculation to improve fidelity. Similarly, the total transformer volume of 1.5 liter is derived from practical core, winding and insulation considerations. No external shell or casing was considered in the weight and volume analysis.

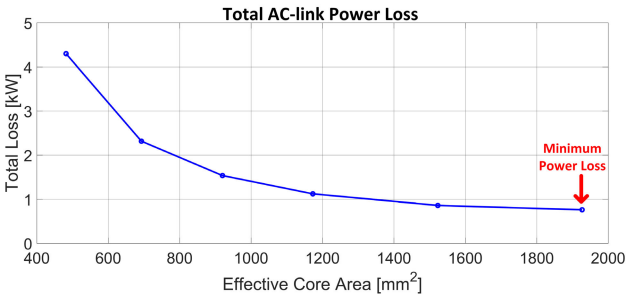

FIGURE 8. Total AC-link power loss including core loss and copper loss.

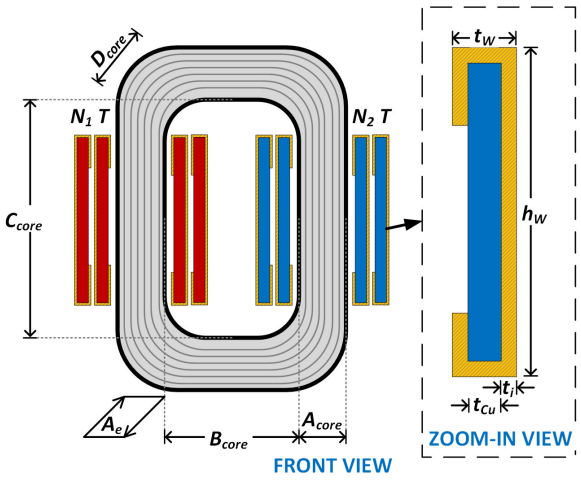

FIGURE 9. Proposed UU core-type transformer design with foil windings.

TABLE 3. Transformer specifications.

Parameter	Symbol	Value
Input Voltage	V_{in}	6 kV
Output Power	P	100 kVA
AC Frequency	f_{ac}	50 kHz
Core Shape		UU
Core Material		F3CC
Core Cross-section Area	A_e	1927 mm^2
Core Window Width	B_{core}	50 mm
Core Window Height	C_{core}	154 mm
Turns Ratio	n	1:1
Number of Turns	$N1, N2$	62 turns
Net Weight		11.7 kg
Volume		1.5 liter
Calculated Core Loss	$Loss_{Fe}$	413 W
Calculated Winding Loss	$Loss_{Cu}$	350 W
Transformer Efficiency	η	99.23 %

IV. EXPERIMENTAL VALIDATION

To validate the loss calculations derived in previous section, a loss measurement testbed is built in the lab. A downscaled testbed is built in the lab with input voltage of 200 V, switching frequency of 40 kHz and AC frequency of 10 kHz. The testbed is configured for two test cases: N = 2 cell/arm and N = 4 cell/arm case to obtain two experimental data points for reliable validation. Ferrite core material 3C81 is used for the transformer prototype. Because this testbed was built to validate the design methodology proposed in this paper rather than to validate any one particular design, the use of a different core material in the testbed from that of the 100 kVA example transformer from Section III is not an issue. The loss calculation is performed based on the specifications of experimental testbed. The testbed along with the circuit diagram showing measurement points is shown in Fig. 10.

$$B(t) = \frac{1}{N_2 \cdot A_e} \int_0^t v(t) dT \tag{10}$$

$$H(t) = \frac{N_1 \cdot i(t)}{l_e} \tag{11}$$

$$P_v = f \oint H \cdot dB \tag{12}$$

The core loss measurements are taken by performing the following steps:

1) The secondary side of the MF transformer is unloaded and voltage and current probes are connected to the testbed to measure the secondary side voltage and primary side current.
2) The transformer's open circuit secondary side voltage measurement is made by a LeCroy differential probe. The primary side transformer current measurement is obtained by using a 50 MHz Yokogawa current probe. Measurements taken are shown in Fig. 11.

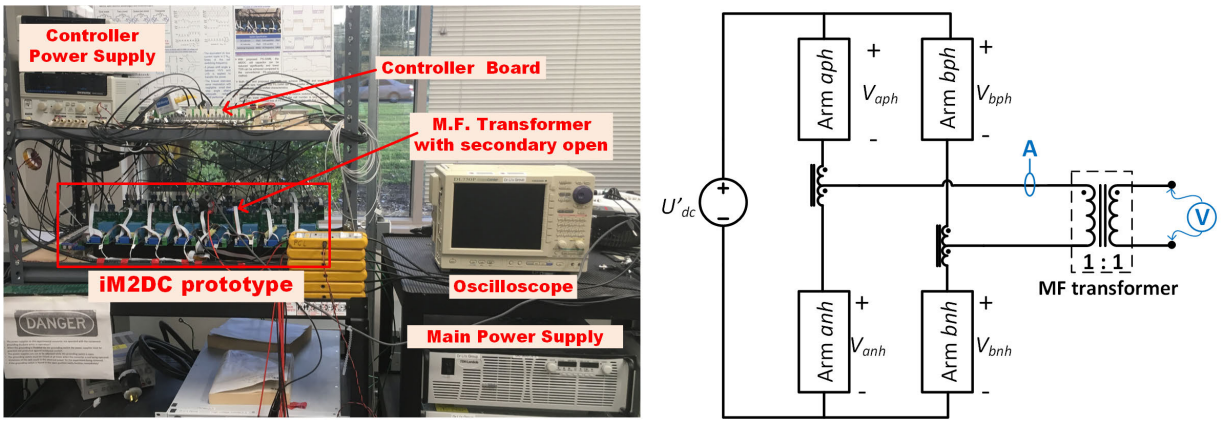

FIGURE 10. MMC module testbed with measurement circuit for N=2;4 cells/arm.

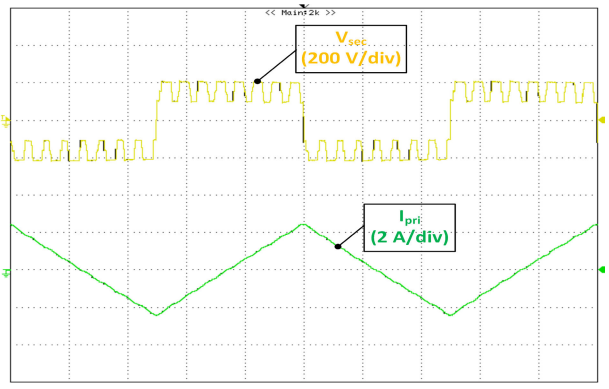

FIGURE 11. Measured voltage and current.

3) The measured quantities are shown in Fig. 11. The measurements are then imported into MATLAB via .csv files and analyzed to determine the magnetizing force (H) and flux density (B).
4) The flux density (B) is calculated from the measurements using Equation (10) [28]. The 1:1 transformer design has 35 turns on each winding and the cross sectional area of the core is 1927 mm^2. The measured and calculated flux densities are found identical as shown in Fig. 12. The solid blue line is from simulation and the red '*' markers are derived from the measurement.
5) The magnetizing force (H) is found by using Equation (11). The magnetic path length of the core l_e is 184 mm.
6) A B-H curve is drawn from the measurements as shown in Fig. 13. The area enclosed by the curve is calculated and the core loss density is found by using Equation (12). The specific core loss can be computed by multiplying the core loss density by the volume of the transformer core which is 290 cubic centimeters.
7) The testbed is reconfigured to N=2 cells/arm to obtain two points of measurement for verification by repeating steps 1-6.

Two sets of results are obtained from two measurement points: N = 2 cells/arm, and N = 4 cells/arm. The results shown in Fig. 11-13 are for the case when N = 4 cells/arm.

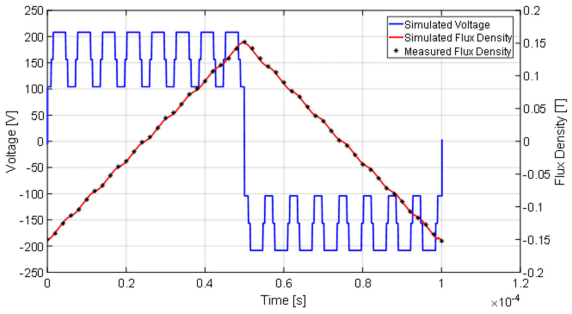

FIGURE 12. Measured and simulated flux densities.

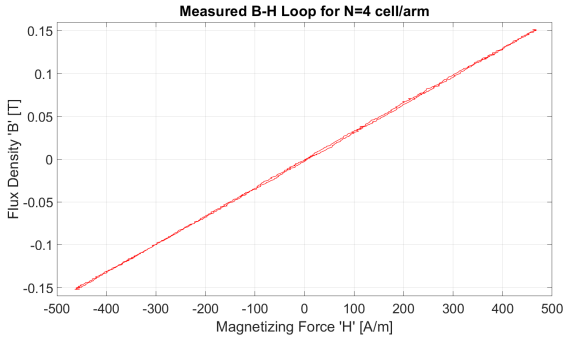

FIGURE 13. B-H loop obtained from measurement.

The calculated and measured results are summarized in Table 4. The calculated and measured core loss densities differ by 10.38% for N = 2 cells/arm case and by 8.05% for N = 4 cells/arm case. It is evident from the results that the iGSE slightly overestimates the losses for the transformer DUT, similar observations were also made in [29]. Measurement noise, curve fitting error in Steinmetz parameter estimation from datasheet and manufacturing tolerances in core geometry are contributing factors to the difference between measured and calculated core loss densities of the MF transformer DUT. Apart from this difference, the core loss calculated with iGSE is consistent with the measurement. This verifies that this method can be used for MF transformer design and optimization of an MMC based solid state transformer module operating with phase shifted square wave modulation.

TABLE 4. Core loss from experiment.

N	Parameter	Value
2	$Area_{B-HLoop}$	2.2627
	$Pv_{measured}$	$22.62 \times 10^3\ W/m^3$
	$Pv_{calculated}$	$25.24 \times 10^3\ W/m^3$
4	$Area_{B-HLoop}$	2.1930
	$Pv_{measured}$	$21.93 \times 10^3\ W/m^3$
	$Pv_{calculated}$	$23.85 \times 10^3\ W/m^3$

V. CORE LOSS UNDER VARYING LOAD CONDITION

In the previous section, the core loss is experimentally measured in no-load condition. The measured core loss is consistent with the calculated core loss, hence the calculation method is validated. In this section, the core loss calculation results for varying load condition and varying flux density is presented. The power transfer in the converter module is controlled by varying the phase shift angle between the primary side and secondary side modulation waves. The current transfer from the primary side to the secondary side is directly proportional to the phase shift angle. Individual flux is generated by the primary and secondary voltages which are superimposed to create the resultant flux as shown in Fig. 14. The shape of the flux in the transformer core is now altered from the no-load flux and the maximum operating flux decreases with the increase in load angle. The core losses for varying flux and load angle is calculated using iGSE hence the losses due to relaxation effect during constant flux density are neglected.

The operating B_{max} at 0° is the condition that needs to be satisfied while selecting the core and winding of the transformer. As the load angle is increased, the operating B_{sat} decreases which slightly lowers the core loss as shown in Fig. 15. A similar observation is also made in [30] for a three phase dual active bridge converter under varying load condition. This effect should be considered while designing the transformer for the MMC based DC-DC converter module to optimize the ideal operating condition.

VI. CONCLUSION

High voltage, isolated DC-DC converters are enablers of future electric network. The MMC module based HVDC-MVDC converter with PS-SWM is a good candidate for HV grid applications, but faces unique challenges in its MF transformer design. This paper proposed a design methodology to solve the unique challenges posed by the MF transformer design, including an accurate method by which to predict the transformer core loss in spite of the atypical nature of the transformer waveforms. The proposed method is validated by a down-scaled experimental testbed operating in two different conditions. The measured loss is found consistent with the predicted loss proving the validity of the proposed core loss estimation method. The winding loss is calculated using Dowell's method for foil conductors and a 100 kVA, 50 kHz transformer is presented with a calculated

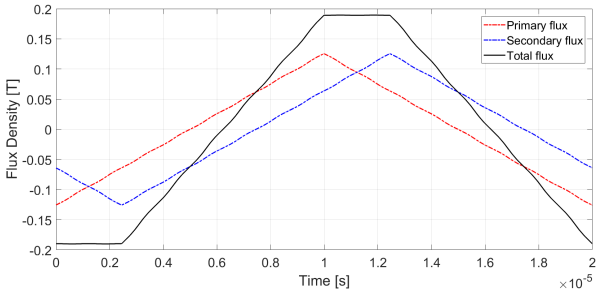

FIGURE 14. Trajectory of flux density for $\phi = 45°$.

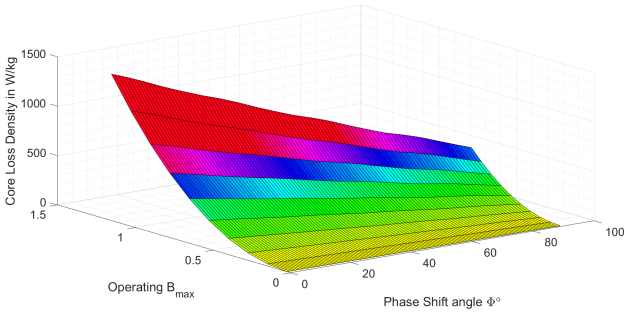

FIGURE 15. Variation of core loss density with flux density and phase angle.

efficiency of 99%. Leveraging the validated core loss estimation method, the core loss for converter operating under variable load is characterized to help identify the specific converter losses under varying operating conditions.

Furthermore, the design considerations and validation of MF transformer loss calculation technique uplifts the technology readiness level of MMC based HVDC-MVDC converters. Some of the other challenges such as improved thermal management of the transformer, standardized insulation design and integration of power transfer impedance into the AC-link needs to be addressed.

REFERENCES

[1] S. Bhattacharya, "Transforming the transformer," *IEEE Spectr.*, vol. 54, no. 7, pp. 38–43, Jul. 2017.

[2] S. Bhattacharya, T. Zhao, G. Wang, S. Dutta, S. Baek, Y. Du, B. Parkhideh, X. Zhou, and A. Q. Huang, "Design and development of generation-I silicon based solid state transformer," in *Proc. 25th Annu. IEEE Appl. Power Electron. Conf. Expo. (APEC)*, Feb. 2010, pp. 1666–1673.

[3] L. Wang, Q. Zhu, W. Yu, and A. Q. Huang, "A medium-voltage medium-frequency isolated DC–DC converter based on 15-kV SiC MOSFETs," *IEEE J. Emerg. Sel. Topics Power Electron.*, vol. 5, no. 1, pp. 100–109, Mar. 2017.

[4] K. Tan, R. Yu, S. Guo, and A. Q. Huang, "Optimal design methodology of bidirectional LLC resonant DC/DC converter for solid state transformer application," in *Proc. IECON-40th Annu. Conf. IEEE Ind. Electron. Soc.*, Oct. 2014, pp. 1657–1664.

[5] I. A. Gowaid, G. P. Adam, A. M. Massoud, S. Ahmed, D. Holliday, and B. W. Williams, "Quasi two-level operation of modular multilevel converter for use in a high-power DC transformer with DC fault isolation capability," *IEEE Trans. Power Electron.*, vol. 30, no. 1, pp. 108–123, Jan. 2015.

[6] S. Cui, N. Soltau, and R. W. De Doncker, "A high step-up ratio soft-switching DC–DC converter for interconnection of MVDC and HVDC grids," *IEEE Trans. Power Electron.*, vol. 33, no. 4, pp. 2986–3001, Apr. 2018.

[7] D. Aggeler and F. Canales, "PE converters and technical challenges for MVDC technologies—DC interlink from decentralized energy sources to HVDC transmission," ABB Switzerland Ltd-Corporate Res., Mar. 2014. [Online]. Available: http://www.apecconf.org/wp-content/uploads/IS2-2-3.pdf
[8] R. Xie, Y. Shi, and H. Li, "Modular multilevel DAB (M2DAB) converter for shipboard MVDC system with fault protection and ride-through capability," in *Proc. IEEE Electric Ship Technol. Symp. (ESTS)*, Jun. 2015, pp. 427–432.
[9] S. Baek and S. Bhattacharya, "Analytical modeling and implementation of a coaxially wound transformer with integrated filter inductance for isolated soft-switching DC–DC converters," *IEEE Trans. Ind. Electron.*, vol. 65, no. 3, pp. 2245–2255, Mar. 2018.
[10] S. Zhao, Q. Li, F. C. Lee, and B. Li, "High-frequency transformer design for modular power conversion from medium-voltage AC to 400 VDC," *IEEE Trans. Power Electron.*, vol. 33, no. 9, pp. 7545–7557, Sep. 2018.
[11] D. Dong, M. Agamy, G. Mandrusiak, and Q. Chen, "Design of high-speed H-bridge converter using discrete SiC MOSFETs for solid-state transformer applications," in *Proc. IEEE Energy Convers. Congr. Expo. (ECCE)*, Oct. 2017, pp. 1379–1386.
[12] S. Kenzelmann, A. Rufer, D. Dujic, F. Canales, and Y. R. de Novaes, "Isolated DC/DC structure based on modular multilevel converter," *IEEE Trans. Power Electron.*, vol. 30, no. 1, pp. 89–98, Jan. 2015.
[13] M. Leibl, G. Ortiz, and J. W. Kolar, "Design and experimental analysis of a medium-frequency transformer for solid-state transformer applications," *IEEE J. Emerg. Sel. Topics Power Electron.*, vol. 5, no. 1, pp. 110–123, Mar. 2017.
[14] R. Mo, H. Li, and Y. Shi, "A phase-shifted square wave modulation (PS-SWM) for modular multilevel converter (MMC) and DC transformer for medium voltage applications," *IEEE Trans. Power Electron.*, vol. 34, no. 7, pp. 6004–6008, Jul. 2019.
[15] R. Mo, R. Xie, Y. Shi, and H. Li, "A PS-SWM strategy for isolated modular multilevel DC/DC converter with reduced passive component size and low total device rating," in *Proc. IEEE Appl. Power Electron. Conf. Expo. (APEC)*, Mar. 2018, pp. 2337–2342.
[16] R. Agarwal, S. Martin, Y. Shi, and H. Li, "High frequency transformer core loss analysis in isolated modular multilevel DC-DC converter for MVDC application," in *Proc. IEEE Energy Convers. Congr. Expo. (ECCE)*, Sep. 2019, pp. 6419–6423.
[17] R. Agarwal, S. Martin, Y. Shi, and H. Li, "High frequency transformer design for medium voltage shipboard DC-DC converter," in *Proc. IEEE Electric Ship Technol. Symp. (ESTS)*, Aug. 2019, pp. 499–504.
[18] B. Zhao, Q. Song, J. Li, Y. Wang, and W. Liu, "High-frequency-link modulation methodology of DC–DC transformer based on modular multilevel converter for HVDC application: Comprehensive analysis and experimental verification," *IEEE Trans. Power Electron.*, vol. 32, no. 5, pp. 3413–3424, May 2017.
[19] Y. Shi and H. Li, "Isolated modular multilevel DC–DC converter with DC fault current control capability based on current-fed dual active bridge for MVDC application," *IEEE Trans. Power Electron.*, vol. 33, no. 3, pp. 2145–2161, Mar. 2018.
[20] W. A. Roshen, "A practical, accurate and very general core loss model for nonsinusoidal waveforms," *IEEE Trans. Power Electron.*, vol. 22, no. 1, pp. 30–40, Jan. 2007.
[21] J. B. Goodenough, "Summary of losses in magnetic materials," *IEEE Trans. Magn.*, vol. 38, no. 5, pp. 3398–3408, Sep. 2002.
[22] *FINEMET F3CC Series Cut Core, 1 2017. T-HT3*, Hitachi Metals, Ltd, Tokyo, Japan, 2017.
[23] R. B. Beddingfield, S. Bhattacharya, and P. Ohodnicki, "Shielding of leakage flux induced losses in high power, medium frequency transformers," in *Proc. IEEE Energy Convers. Congr. Expo. (ECCE)*, Sep. 2019, pp. 4154–4161.
[24] K. Venkatachalam, C. R. Sullivan, T. Abdallah, and H. Tacca, "Accurate prediction of ferrite core loss with nonsinusoidal waveforms using only Steinmetz parameters," in *Proc. IEEE Workshop Comput. Power Electron.*, Jun. 2002, pp. 36–41.
[25] C. W. T. McLyman, *Transformer and Inductor Design Handbook*, 4th ed. Boca Raton, FL, USA: CRC Press, 2011.
[26] P. L. Dowell, "Effects of eddy currents in transformer windings," *Proc. Inst. Electr. Eng.*, vol. 113, no. 8, pp. 1387–1394, Aug. 1966.
[27] M. A. Bahmani, T. Thiringer, and H. Ortega, "An accurate pseudoempirical model of winding loss calculation in HF foil and round conductors in switchmode magnetics," *IEEE Trans. Power Electron.*, vol. 29, no. 8, pp. 4231–4246, Aug. 2014.
[28] J. Muhlethaler, J. Biela, J. W. Kolar, and A. Ecklebe, "Improved core-loss calculation for magnetic components employed in power electronic systems," *IEEE Trans. Power Electron.*, vol. 27, no. 2, pp. 964–973, Feb. 2012.
[29] N. Soltau, D. Eggers, K. Hameyer, and R. W. De Doncker, "Iron losses in a medium-frequency transformer operated in a high-power DC–DC converter," *IEEE Trans. Magn.*, vol. 50, no. 2, pp. 953–956, Feb. 2014.
[30] S. Cui, N. Soltau, and R. W. De Doncker, "A high step-up ratio soft-switching DC-DC converter for interconnection of MVDC and HVDC grids," in *Proc. IEEE Energy Convers. Congr. Expo. (ECCE)*, Sep. 2016, pp. 1–8.

RACHIT AGARWAL (Student Member, IEEE) received the bachelor's degree in electrical engineering from Uttar Pradesh Technical University (now AKTU), India, in 2014, and the M.S. degree in electrical engineering from Florida State University (FSU), Tallahassee, FL, USA, in 2018, where he is currently pursuing the Ph.D. degree with the Center for Advanced Power Systems, conducting research in topology, modeling, and control of high voltage power electronics. His research interests include isolated dc–dc converters, WBG based solid state transformers, and multilevel converters.

SANDRO MARTIN (Student Member, IEEE) received the B.S. and Ph.D. degrees in electrical engineering from Florida State University, Tallahassee, FL, USA. Since May 2016, he has been with the Center for Advanced Power Systems, Florida State University. From May 2018 to September 2018, he was an Electrical Engineering Intern with Mainstream Engineering Corporation. His research interests include modeling and control, modular multilevel converters, and DC solid-state transformers.

HUI LI (Fellow, IEEE) received the B.S. and M.S. degrees from the Huazhong University of Science and Technology, Wuhan, China, in 1992 and 1995, respectively, and the Ph.D. degree from the University of Tennessee, Knoxville, TN, USA, in 2000, all in electrical engineering.

She is currently a Professor with the Department of Electrical and Computer Engineering, Florida A&M University—Florida State University College of Engineering, Tallahassee, FL, USA. Her current research interests include PV converters, energy storage applications, and smart grid.